

Diagnosing ablator ρR and ρR asymmetries in capsule implosions using charged-particle spectrometry at the National Ignition Facility

J. A. Frenje,¹ C. K. Li,¹ J. R. Rygg,^{1,a)} F. H. Séguin,¹ D. T. Casey,¹ R. D. Petrasso,^{1,b)} J. Delettrez,² V. Yu. Glebov,² T. C. Sangster,² O. Landen,³ and S. Hatchett³

¹*Plasma Science and Fusion Center, Massachusetts Institute of Technology, Cambridge, Massachusetts 02139, USA*

²*Laboratory for Laser Energetics, University of Rochester, Rochester, New York 14623, USA*

³*Lawrence Livermore National Laboratory, Livermore, California 94550, USA*

(Received 26 February 2008; accepted 9 July 2008; published online 24 February 2009)

By fielding several compact proton spectrometers at various locations around an ignition-capsule implosion at the National Ignition Facility [G. H. Miller, E. I. Moses, and C. R. Wuest, *Nucl. Fusion* **44**, S228 (2004)], ρR and ρR asymmetries of the ablator for a failed implosion can be obtained through absolute measurements of knock-on proton (KO-P) spectra. For ignition capsules with a Cu-doped beryllium (Be) ablator, 50:50 mixture of deuterium-tritium (DT) fuel and $\sim 1\%$ residual hydrogen (H) by atom, failed implosions can be diagnosed for neutron yields ranging from $\sim 10^{11}$ to $\sim 6 \times 10^{15}$ and local ρR s up to ~ 240 mg/cm². For capsules with an ablator of Ge-doped CH, which contains a large amount of H, failed implosions can be diagnosed for neutron yields ranging from $\sim 10^{10}$ to $\sim 6 \times 10^{15}$ and local ρR s up to ~ 200 mg/cm². Prior to the first ignition experiments, capsules with a Cu-doped Be ablator (or Ge-doped CH ablator), more deuterium-lean fuel mixture and H-dopant levels up to 25% in the fuel will be imploded to primarily reduce the neutron yield. The HDT-filled Be-capsule implosion, which can be diagnosed for neutron yields ranging from $\sim 5 \times 10^9$ to $\sim 6 \times 10^{15}$ and local ρR s up to ~ 240 mg/cm², is more suitable to diagnose using KO-Ps as the signal-to-background ratio is significantly higher than for an ignition-capsule implosion. In addition, analysis of CH-ablator data obtained from analogous OMEGA [T. R. Boehly, D. L. Brown, R. S. Craxton *et al.*, *Opt. Commun.* **133**, 495 (1997)] experiments indicate that the shape of the KO-P spectrum is affected mainly by the ablator ρR . Other effects such as ablator-density-profile variations, time evolution of the ablator ρR , fuel-ablator mix and electron temperature variations typically predicted for the ablator play minor roles. © 2009 American Institute of Physics. [DOI: 10.1063/1.2965829]

I. INTRODUCTION

Ignition of an indirectly laser-driven capsule implosion at the National Ignition Facility (NIF) (Ref. 1) requires careful tuning of the drive conditions to the capsule parameters.²⁻⁵ Inadequate knowledge about the drive physics is therefore a serious concern, since an underdriven or overdriven capsule will leave too much or too little ablator mass as payload and thus reduce the performance of an implosion to the point it fails to ignite.² If the initial ablator is too thin, it burns through too quickly and the implosion fails to ignite due to preheat or instability issues; or if the initial ablator is too thick, the implosion velocity is too low and the implosion fails to ignite due to poor compression. To address this issue, we propose to accurately diagnose the areal density (ρR) of the ablator using charged-particle spectrometry. By fielding several compact charged-particle spectrometers (spectrometer housing is less than 5 cm in diameter)⁶ at various locations around a NIF implosion, ρR and ρR asymmetries of the ablator can be obtained through measurements of spectra of knock-on protons (KO-P) elastically scattered by primary

DT neutrons.⁷ The KO-Ps have a well known, flat birth spectrum ranging from 0 to 14 MeV, and as they traverse through the ablator they lose energy in proportion to the amount of material they pass through (ρR). A ρR value for the portion of the implosion facing a given spectrometer can therefore be determined from the energy downshift and shape of the measured KO-P spectrum by applying a newly developed analysis technique, which utilizes Monte Carlo modeling⁸ of an implosion and the plasma-stopping power formalism described in Ref. 9. Using this technique, it is shown in this work that the shape of the spectrum of the escaping KO-Ps can be used to accurately diagnose a variety of ablator compositions for neutron yields up to $\sim 6 \times 10^{15}$ and ablator ρR s up to ~ 240 mg/cm² (Ref. 10).

The work described herein improves and extends significantly the work by Nakaishi *et al.*,¹¹ Li *et al.*,¹² and Frenje *et al.*,¹³ who used a relatively simple implosion model to relate the ρR to the measured KO-P yield. Nakaishi *et al.* applied the yield method to a coarse KO-P spectrum measured in a single direction for a thin-glass microballoon capsule implosion; while Li *et al.* and Frenje *et al.* used the yield method to infer a fuel ρR from high-resolution KO-P spectra obtained simultaneously in several different directions for ICF-relevant capsule implosions. However, as noted by Frenje

^{a)}Present address: Lawrence Livermore National Laboratory, Livermore, California 94550, USA.

^{b)}Also Visiting Senior Scientist, Laboratory for Laser Energetics at the University of Rochester, Rochester, New York 14623, USA.

et al., this yield method is subject to significant spatial-yield variations, most likely caused by magnetic fields surrounding an implosion prohibiting ρR asymmetries to be diagnosed. As a result, only an average ρR can be obtained from several spectrometers fielded around an implosion using this method. In this context, it is also important to note that Seguin *et al.*¹⁴ and Hicks *et al.*¹⁵ demonstrated that the energies of the KO-Ps are not affected when bang time occurs after the laser pulse (when the electrical field has decayed away). This is also the case for the NIF-capsule implosions discussed in this work. According to simulations, the bang time for these implosions occurs typically a nanosecond after the laser pulse has been turned off. Measurement of the KO-P spectrum is therefore a much more powerful method than the yield method for diagnosing the ablator ρR of a capsule implosion at the NIF, and in general.

In addition, the KO-P measurements and analysis technique described herein will nicely complement and extend the work by Wilson *et al.*,¹⁶ Hicks *et al.*,¹⁷ and Olson *et al.*^{18,19} that were carried out mainly at the OMEGA laser facility. Wilson *et al.* applied a technique, extensively used at OMEGA for the last decade,^{6,14,20} to determine the ρR of the ablator from the energy downshift of 14.7-MeV protons produced in surrogate D^3He gas-filled CH-capsule implosions; Hicks *et al.* implemented an x-ray radiography technique that measures time-resolved ρR , mass, and velocity of the ablator; and Olson *et al.* studied x-ray ablation rates in planar geometries for Cu-doped Be, high density carbon, and Ge-doped CH, among other materials. All these techniques have distinctly different but complementary strengths.

This paper is structured as follows: Secs. II and III describe the methods for diagnosing the ablator ρR in several types of NIF-capsule implosions, while Sec. IV describes the proposed ablator ρR measurements at the NIF. Section V discusses KO-P measurements performed at OMEGA, similar in spirit to those proposed herein for the NIF. Section VI summarizes the main results.

II. DIAGNOSING THE ABLATOR ρR IN IGNITION-CAPSULE IMPLOSIONS

The current design of the 285 eV indirect-drive ignition capsule consists of a cryogenic deuterium-tritium (DT) layer of 75 μm with the outer surface positioned at a radius of 1000 μm . The capsule, which is filled with DT gas in equilibrium at 0.3 mg/cm^3 , has an outer ablator layer with thickness varying from 90 to 170 μm depending on the ablator composition. At least three ablator designs are under consideration.^{3,4,21–25} The first design is made of beryllium (Be), doped gradually with copper; the second design is made of CH, doped gradually with germanium; the third design, which is not discussed in this paper, is made of high-density carbon.

Diagnosing the Be-ablator design can be done by utilizing the $\sim 1\%$ residual H (by atom) in the DT fuel, and measure the energy spectrum of the KO-Ps produced in the fuel. As the KO-Ps produced in the fuel at the fuel-Be-ablator interface lose the least amount of energy, the high-energy endpoint of the KO-P spectrum provides accurate informa-

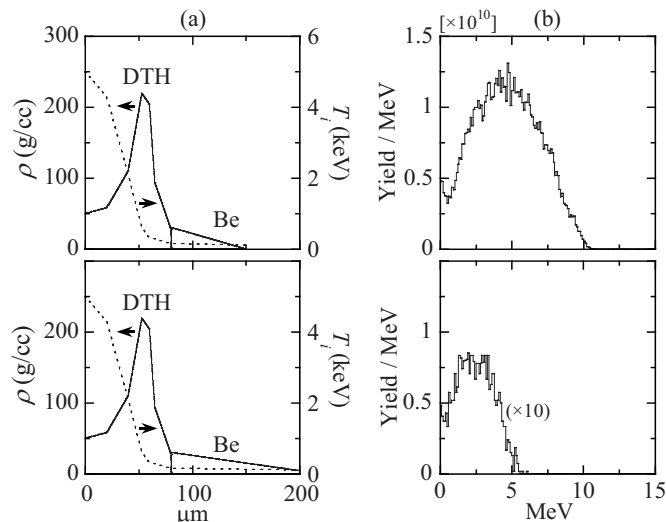


FIG. 1. Simulations of two Be-capsule implosions. (a) Same density and temperature profiles were used for the fuel, while different density profiles were used for the Be ablator, i.e., the ablator extended out to a radius of 150 μm (top figure) and 220 μm (bottom figure) corresponding to an ablator ρR of 105 mg/cm^2 and 210 mg/cm^2 , respectively. These numbers are equivalent to a mass of $\sim 150 \mu\text{g}$ and $\sim 440 \mu\text{g}$, respectively, which can be contrasted to a fuel mass of $\sim 240 \mu\text{g}$. DT fuel with $\sim 1\%$ of residual hydrogen (by atom) was used in the simulations. A primary neutron yield of 5.3×10^{15} was computed for both implosions. (b) Simulated KO-P spectra for the two implosions. A high-energy endpoint at 10 MeV (top figure) and 6 MeV (bottom figure) was simulated for the implosion with an ablator ρR of 105 mg/cm^2 and 210 mg/cm^2 , respectively. Only a small fraction of the produced KO-Ps exit the Be ablator; $\sim 8 \times 10^{10}$ KO-Ps exit the 105 mg/cm^2 ablator, and $\sim 3 \times 10^9$ KO-Ps exit the 210 mg/cm^2 ablator. These KO-Ps are born in the $\sim 30 \mu\text{m}$ and $\sim 10 \mu\text{m}$ outermost region of the fuel for the 105 mg/cm^2 and 210 mg/cm^2 ablator case, respectively. In addition, a decreasing KO-P yield with decreasing energy is observed at lower energies. This is caused by an increasing fraction of ranged out KO-Ps as the birth energy of these protons decreases. The KO-Ps are fully ranged out at a Be ablator ρR of $\sim 260 \text{mg}/\text{cm}^2$.

tion about the ρR of the remaining Be ablator. To quantitatively study how the Be ablator affects the KO-P spectrum, a Monte Carlo code⁸ was used to simulate burn-averaged KO-P spectra for two capsule implosions that are similar to the failed one described in Ref. 26. The density and temperature profiles of the fuel and Be ablator used in the simulations are illustrated in Fig. 1(a). As shown by Fig. 1(a), the density and temperature profiles for the fuel were kept the same, while the density profile for the Be ablator was changed artificially to illustrate the effect of a varying ρR on the KO-P high-energy endpoint. In the simulations, the ablator profile extends out to a radius of 150 μm (top figure) and to a radius of 220 μm (bottom figure) corresponding to an ablator ρR of 105 mg/cm^2 and 210 mg/cm^2 , respectively. The resulting simulated KO-P spectra, shown in Fig. 1(b), indicate high-energy endpoints at 10.0 MeV and 6.0 MeV, and thus energy downshifts of 4.0 MeV and 8 MeV for the 105 mg/cm^2 and 210 mg/cm^2 ablator, respectively. From these numbers, it is evident that the energy downshift depends strongly on ρR and can be used to accurately infer the ρR of the remaining Be ablator.²⁷ This strong relationship is also illustrated in detail by the filled circles in Fig. 2, which are the results from several simulations. As shown by these

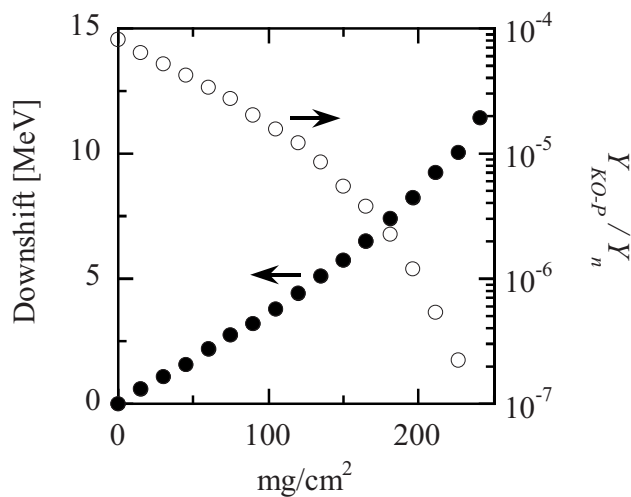


FIG. 2. Simulated energy downshift (●) and $Y_{\text{KO-P}}/Y_n$ ratio (○) as a function of ρR of the remaining Be ablator. The density and temperature profiles of the fuel were kept constant in these simulations [see Fig. 1(a)], while the density profile and thus ρR of the ablator was changed artificially. As the ablator ρR increases from zero to ~ 250 mg/cm², the $Y_{\text{KO-P}}/Y_n$ ratio decreases several orders of magnitude. A primary neutron yield of 5.3×10^{15} was simulated for these implosions.

data points, the Be ablator can be diagnosed for ρR s up to ~ 240 mg/cm².

Electron temperature (T_e) variations typically predicted in the ablator do not significantly affect the ρR inferred from the energy downshift of the KO-*P*s. To change the inferred ablator ρR value by only 1%, one has to change T_e in the analysis from ~ 100 eV to an unreasonable value of ~ 1000 eV. Measuring the high-energy end point of the KO-*P* spectrum is therefore a sensitive and weakly model dependent method for determining the ρR of the remaining Be ablator.

As shown in Fig. 1(b), a much larger fraction of the produced KO-*P*s exit the 105 mg/cm² ablator than the 210 mg/cm² ablator; $\sim 8 \times 10^{10}$ KO-*P*s exit the 105 mg/cm² ablator, while only $\sim 3 \times 10^9$ KO-*P*s exit the 210 mg/cm² ablator, which corresponds to a KO-*P*s to neutron yield ratio ($Y_{\text{KO-P}}/Y_n$) of $\sim 1.5 \times 10^{-5}$ and $\sim 5.7 \times 10^{-7}$, respectively. These KO-*P* protons are born in the ~ 30 μm and ~ 10 μm outermost regions of the fuel for the 105 mg/cm² and 210 mg/cm² ablator cases, respectively. The exact trend of how the $Y_{\text{KO-P}}/Y_n$ ratio varies with increasing ρR of the Be ablator is illustrated by the open circles in Fig. 2. In addition, it should be noted that due to the build up of ³He in the fuel, these KO-*P* measurements could in principle be affected by 14.7 MeV D³He protons. However, simulations indicate that the D³He protons are fully ranged out as they are produced in the innermost 40–50 μm in the fuel (due to the strong temperature dependence of the D³He fusion reaction). As a result, the D³He protons do not affect the KO-*P* measurements.

The CH-ablator design, which contains naturally large amounts of H, can be diagnosed by measuring the absolute spectrum of KO-*P*s produced in the ablator. In particular, the shape of the measured KO-*P* spectrum provides information about the ablator ρR . This is illustrated in Fig. 3, which

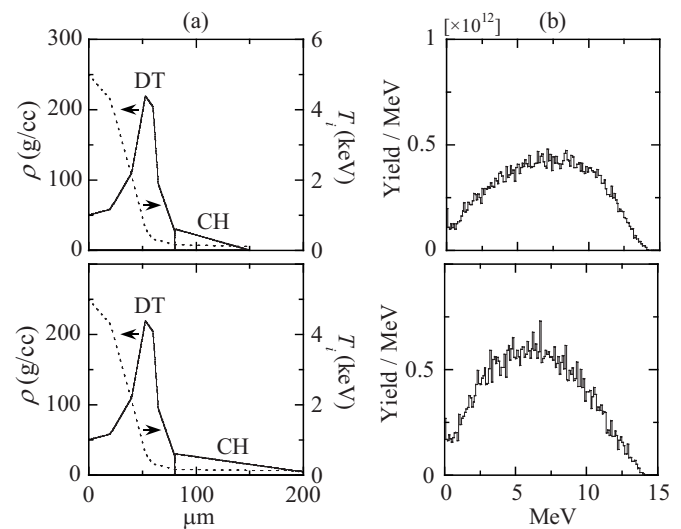


FIG. 3. Simulations of two CH-capsule implosions. (a) Same density and temperature profiles were used for the fuel, while different density profiles were used for the CH ablator, i.e., the ablator extended out to a radius of 150 μm (top figure) and 220 μm (bottom figure) corresponding to an ablator ρR of 105 mg/cm² and 210 mg/cm², respectively. Both implosions produced 5.3×10^{15} primary neutrons. (b) Simulated KO-*P* spectra for the two implosions. These spectra indicate clearly that the shape can be used to diagnose the ρR of the CH ablator. An average ρR of the ablator can also be inferred from the KO-*P* yield as described by Eq. (1). For the 105 mg/cm² and 210 mg/cm² case, a total KO-*P* yield of 4×10^{12} (top figure) and 6×10^{12} (bottom figure) was simulated, respectively.

shows simulations of two capsule implosions. The density and temperature profiles used for the fuel and ablator in these two simulations are shown in Fig. 3(a). Once again, the density and temperature profiles for the fuel were kept the same, while the density profile for the ablator was changed artificially to illustrate the effect of a varying ρR on the shape of the KO-*P* spectrum. In the simulations, the ablator extends out to a radius of 150 μm (top figure) and 220 μm (bottom figure) corresponding to an ablator ρR of 105 mg/cm² and 210 mg/cm², respectively. The resulting KO-*P* spectra, shown in Fig. 3(b), indicate that the change of the ablator ρR has a significant impact on the shape of the KO-*P* spectrum. In contrast, the shape of the KO-*P* spectrum is not affected significantly by ablator-density-profile variations even though the spatial birth profile of the KO-*P*s depends strongly on the density profile. This is a consequence of the fact that the energy-slowing down of the KO-*P*s is very weakly dependent on mass-density-profile variations. As shown in the references,⁶ the energy-slowing down depends mainly on ρR , while density and temperature effects play minor roles. Other effects, such as time evolution of the ablator ρR and fuel-shell mix play minor roles as well, as described in more detail in the next two paragraphs.

The time evolution of the ablator ρR does not affect significantly the shape of the KO-*P* spectrum, which significantly simplifies the interpretation of the measured KO-*P* spectrum. This is illustrated by transporting KO-*P*s through density and temperature profiles simulated by the 1D hydrocode LILAC,²⁸ at different times for a hydroequivalent capsule implosion at OMEGA. It is meaningful to use this type of implosion to study how the time-evolution of the ablator

ρR affects the KO-P spectrum for an ignition-scaled NIF-capsule implosion as the burn duration and percentage variation of the ablator ρR during burn are similar for these implosions. The density and temperature profiles used in this exercise are illustrated in Figs. 4(a) and 4(b), which show the density and temperature profiles at bang time (BT), BT - 100 ps, and BT + 80 ps for an imploding DT-gas filled CH capsule at OMEGA (a total burn duration of ~ 180 ps was simulated for this particular implosion). The resulting KO-P spectra for the different times are shown in Fig. 4(c). Each simulated KO-P spectrum was determined assuming a steady-state condition for 60 ps. Despite the fact that KO-Ps are produced before and after bang time, the KO-P spectrum produced at bang time dominates and well represents the burn-weighted spectrum; an indication that a time-integrated measurement of the KO-P spectrum will provide accurate information about the ablator ρR at bang time.

Fuel-ablator mix also plays a minor role. As the fuel density and temperature is much lower in the mixed region than in the clean region, the radial source profile of the primary neutrons is not affected by mix to a level that the KO-P spectrum is significantly altered. However, the fuel-ablator mix does alter the ablator-density-profile, but this has no impact on the shape of the KO-P spectrum as already discussed.

Although $Y_{\text{KO-P}}$ is subject to significant spatial-yield variations, most likely caused by magnetic fields surrounding an implosion, an average $Y_{\text{KO-P}}$ determined from several measurements can be used to infer a spatially averaged ρR of the CH ablator as discussed in Refs. 12 and 13. By using a relatively simple model of an implosion, the $Y_{\text{KO-P}}$, normalized to the neutron yield Y_n , can be related to the ablator ρR by

$$\frac{Y_{\text{KO-P}}}{Y_n} = \frac{\gamma \sigma_p}{(\gamma + 12) m_p} \xi(\rho R) \rho R, \quad (1)$$

where $\gamma = n_H/n_C$ ($\gamma \approx 1.4$ for CH); σ_p is the total cross section for the np -elastic scattering process; m_p is the proton mass; and $\xi(\rho R)$ is a function describing the fraction of escaping KO-Ps. Typically ~ 200 mg/cm² of the ablator ρR remain at bang time for an over-driven capsule implosion, which would generate a KO-P yield of $\sim 10^{-3} \times Y_n$. As $Y_{\text{KO-P}}$ is directly proportional to $\rho R \cdot Y_n$, and the ablator ρR and Y_n are strong functions of the laser drive (a 30%–40% variation in the laser drive changes the ablator ρR by a factor of ~ 2 and the Y_n by at least a factor of 10), measurements of $Y_{\text{KO-P}}$ should allow studies of the ablator ρR and the drive-physics. To understand quantitatively how the $Y_{\text{KO-P}}/Y_n$ ratio varies with the ρR of the remaining CH ablator, several simulations of a capsule implosion were performed. In the simulations, the same density and temperature profiles of the fuel were used as for the capsule implosions shown in Fig. 3(a), while the profile of the CH ablator was changed artificially. The resulting data from these simulations, which are shown in Fig. 5, indicate that the $Y_{\text{KO-P}}/Y_n$ ratio (filled circles) saturates at $\sim 10^{-3}$ for ρR 's above 150 mg/cm². In addition, the escaping fraction reduces from 50% to 10% (relative to the number of produced KO-Ps) as the ρR increases from prac-

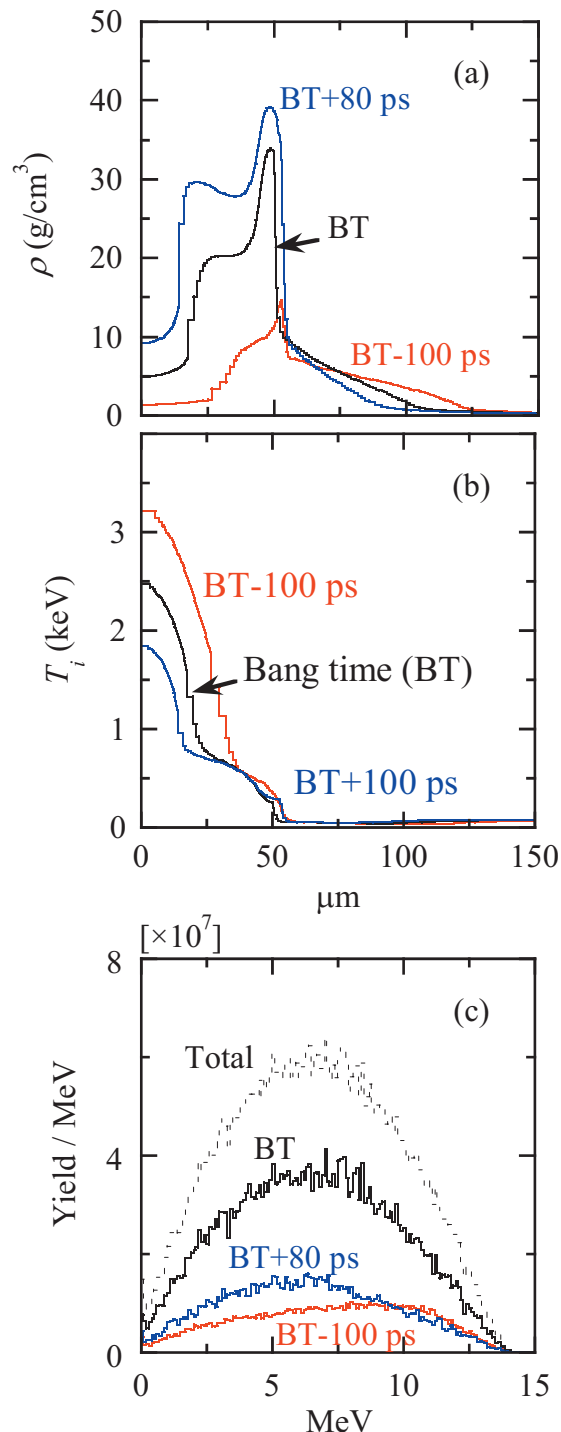


FIG. 4. (Color) (a) Simulated LILAC density profiles at three different times, i.e., at bang time (BT), BT - 100 ps, and BT + 80 ps for OMEGA shot 39894 (an imploding 3-atm DT filled 27 μm thick CH capsule, which is discussed in more detail in Sec. V). A total burn duration of ~ 180 ps (FWHM) was simulated for this particular shot when using a flux limiter of 0.06. (b) Corresponding simulated temperature profiles. (c) Simulated KO-P spectra for the three different times (each simulated spectrum was computed assuming a steady-state condition for 60 ps). Also shown in (c) is the total, burn-weighted KO-P spectrum that is very similar in shape to the spectrum produced at bang time, indicating that the time evolution of the ablator ρR plays a minor role in the ρR analysis of the measured KO-P spectrum.

tically zero to ~ 250 mg/cm². Very relevant to this discussion is that these measurements are not affected significantly by the KO-Ps produced in the fuel (due to the $\sim 1\%$ residual H) as the yield of the escaping KO-Ps, produced in the fuel,

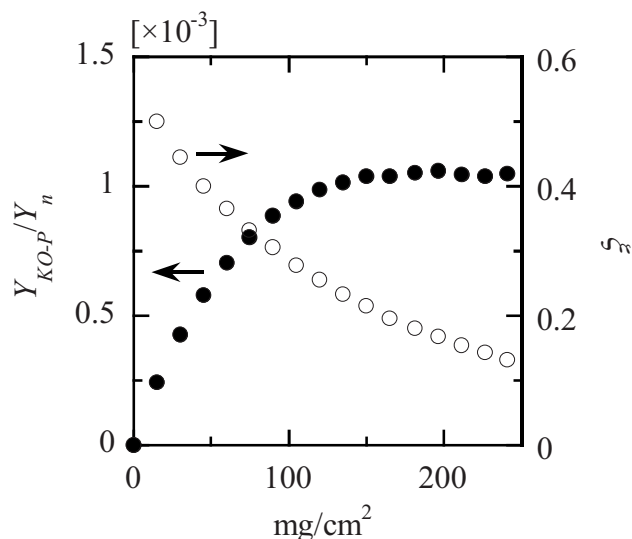


FIG. 5. Simulated $Y_{\text{KO-P}}/Y_n$ ratio (●) and KO-P escaping fraction (○), ξ , as a function of ρR of the CH ablator. The density and temperature profiles of the fuel were kept constant [see Fig. 3(a)] in these simulations, while the density profile and thus ρR of the ablator was changed artificially. As shown, the yield ratio saturates at ~ 150 mg/cm² and the escaping fraction ξ decreases from $\sim 50\%$ to $\sim 10\%$ as the ablator ρR increases from zero to ~ 250 mg/cm².

is typically orders of magnitude lower than the yield of the escaping KO-Ps produced in the CH ablator (this is understood qualitatively when comparing the data in Figs. 2 and 5). Even at very low ablator ρR s, the number of escaping KO-Ps coming from the CH ablator dominates the number of escaping KO-Ps coming from the fuel. As a result, the measured $Y_{\text{KO-P}}/Y_n$ ratio can be used to diagnose the CH ablator for ρR s up to ~ 150 mg/cm².

III. DIAGNOSING THE ABLATOR ρR IN IMPLODING CAPSULES FILLED WITH HYDROGEN-DEUTERIUM-TRITIUM (HDT) FUEL

Prior to the first ignition experiments, capsules with a Cu-doped Be ablator (or Ge-doped CH ablator), more deuterium-lean fuel mixtures and H-dopant levels up to 25% (by atom) in the fuel will be imploded to primarily reduce the primary neutron yield. To keep these implosions hydrodynamically equivalent to an ignition-capsule implosion, and to maintain the cryogenic tritium fuel layering capabilities, stringent requirements on the fuel composition are applied. Two examples of deuterium-lean fuel compositions that are being considered are 22% H: 8% D: 70% T and 25% H: 0.5% D: 75% T. With a significantly higher H content in the fuel than in the ignition-capsule implosion, the HDT-filled Be-capsule implosions are more suitable to diagnose using KO-Ps as $Y_{\text{KO-P}}$ increases and Y_n decreases resulting in a significantly higher signal-to-background (S/B) ratio.²⁹ This is also illustrated in Fig. 6, which shows simulated KO-P

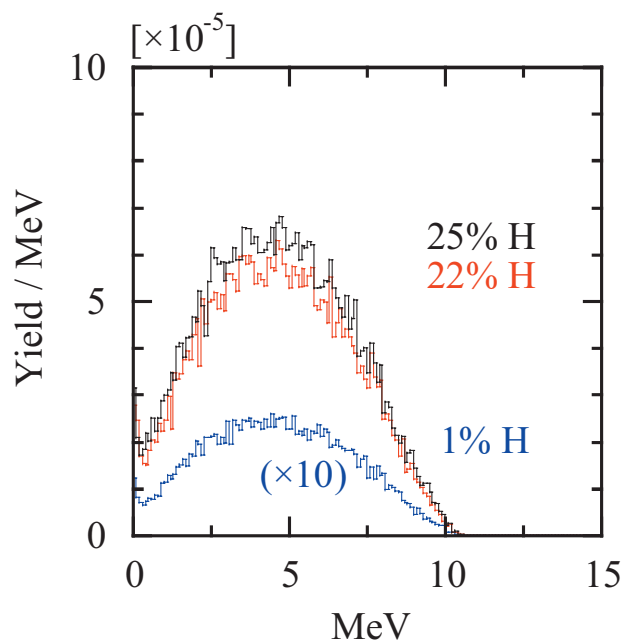


FIG. 6. (Color) Simulated KO-P spectra normalized by Y_n for a Cu-doped Be ablator and DT fuel doped with 22% and 25% H (red and black lines). For comparison, the normalized KO-P spectrum for the failed ignition-capsule implosion is also shown (blue line). To maintain hydrodynamic equivalence to the ignition-capsule implosion, the fuel composition of the H-filled Be-capsule implosions are 22% H: 8% D: 70% T: and 25% H: 0.5% D: 75% T. The same density and temperature profiles were used in all these simulations [see Fig. 1(a), top graph]. Primary neutron yields of 1.2×10^{15} and 7.9×10^{13} were simulated for the 22%-H-filled and 25%-H-filled Be-capsule implosions, respectively. Although these primary neutron yields are ~ 4.5 times and ~ 66 times lower than for the failed ignition-capsule implosion, $Y_{\text{KO-P}}$ is in fact ~ 5 times higher (4.5×10^{11}) and only ~ 2.5 times lower (3.3×10^{10}) for the 22%-H-filled and 25%-H-filled Be-capsule implosions, respectively. As a result, the signal-to-background (S/B) ratios are improved significantly as discussed in Secs. III and IV. The same high-energy endpoint of 10 MeV was simulated in all three cases, which involved a 105 mg/cm² Be ablator.

spectra (normalized by Y_n) for the 22%-H-filled and 25%-H-filled Be-capsule implosions, and for the failed ignition-capsule implosion. Even though the simulated Y_n for the 22%-H-filled and 25%-H-filled Be-capsule implosion is ~ 4.5 and ~ 66 lower, respectively, than for the failed ignition-capsule implosion, the KO-P yield is in fact ~ 5 times higher and only ~ 2.5 times lower, respectively. As a result, the S/B ratio is 22 and 25 times higher for the 22%-H-filled and 25%-H-filled Be-capsule implosions, respectively, than for the failed ignition-capsule implosion. Further discussions about the absolute S/B ratios can be found in the next section. In addition, as the Be-ablator profile is identical for these capsule implosions, the same high-energy endpoint of 10 MeV was simulated.

IV. PROPOSED ABLATOR ρR MEASUREMENTS AT THE NIF

The plan is to field several compact CR-39 based proton spectrometers (the spectrometer housing is less than 5 cm in diameter)⁶ at various locations around an implosion to diagnose ρR and ρR asymmetries of the remaining ablator at bang time. As the CR-39 efficiency for detecting KO-Ps and background neutrons is 100% and $\sim 6 \times 10^{-5}$,³⁰ respectively,

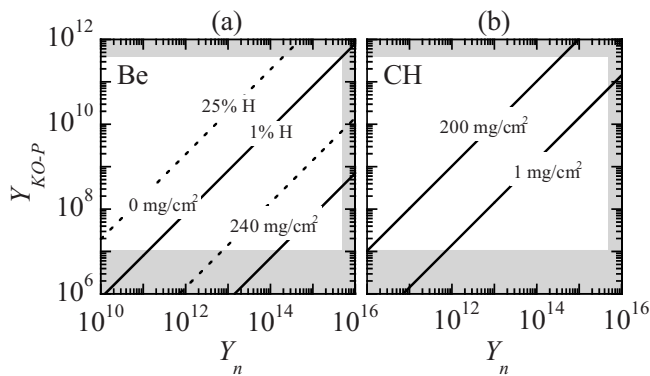


FIG. 7. (a) Absolute $Y_{\text{KO-P}}$ as a function of Y_n and ρR for ignition-capsule implosions with $\sim 1\%$ residual H (solid lines) and 25%-H-filled Be-capsule implosions (dashed lines). (b) Absolute $Y_{\text{KO-P}}$ as a function of Y_n and ρR for CH-capsule implosions. In contrast to the Be-ablator data, $Y_{\text{KO-P}}$ increases with increasing ρR . The white areas in both graphs indicate the measurable $Y_{\text{KO-P}}$ and Y_n ranges at the NIF. In both figures, the lower and upper limits of the measurable ρR 's are also indicated.

the dynamic range of the spectrometer is determined mainly by the allowed range of spectrometer distances to the implosion, signal statistics, and signal saturation. About $\sim 10^3$ signal counts are required for inferring an ablator ρR from either the high-energy end point or the shape of the KO-P spectrum, and $\sim 10^5$ signal counts per cm^2 are required for the CR-39 to saturate.⁶ With an active spectrometer area of 2 cm^2 , a range of allowed spectrometer distances of 40–550 cm to the implosion and $1/R^2$ -scaling of the detected KO-P signal, absolute spectra can be measured accurately for a $Y_{\text{KO-P}}$ ranging from $\sim 1 \times 10^7$ to $\sim 4 \times 10^{11}$. This absolute yield range combined with the simulated results shown in Figs. 2 and 5, which illustrate the $Y_{\text{KO-P}}/Y_n$ ratio as a function of the ablator ρR , is used to establish the absolute KO-P yield as a function of Y_n and ρR for the different ablators (see Fig. 7). The Be-ablator curves, shown in Fig. 7(a), indicate a tolerable Y_n ranging from $\sim 5 \times 10^9$ to $\gg 10^{16}$ [the solid and dashed line is for the failed ignition-capsule implosion (with $\sim 1\%$ residual H) and 25%-H-filled Be-capsule implosion, respectively]. However, as the ρR of the Be ablator approaches $240 \text{ mg}/\text{cm}^2$, $Y_{\text{KO-P}}$ decreases significantly to the point where the S/B ratio is well below one. At this point, the CR-39 saturation is dictated by the neutron background. Based on the information in Ref. 30, an upper Y_n limit of $\sim 6 \times 10^{15}$ is determined for a spectrometer positioned at 550 cm to the implosion. Similar arguments can be applied to the CH-ablator case, resulting in a tolerable Y_n ranging from $\sim 10^{10}$ to $\sim 6 \times 10^{15}$ as shown in Fig. 7(b).

Maximizing the S/B ratio is essential to the proposed KO-P measurements. Using a standard-counting technique (SCT),⁶ utilized for more than a decade, about an order of magnitude background reduction is achieved, resulting in a S/B range of ~ 0.01 –10 and ~ 0.2 –200 for the failed ignition-capsule implosion and 25%-H-filled Be-capsule implosion, respectively [see Fig. 8(a)]. In the case of the CH ablator, the S/B varies from ~ 1 to ~ 100 as illustrated in Fig. 8(b). In both cases, the S/B is independent of Y_n and only varies with varying ablator ρR . By applying the coincidence-counting technique (CCT) (Refs. 31 and 32) to

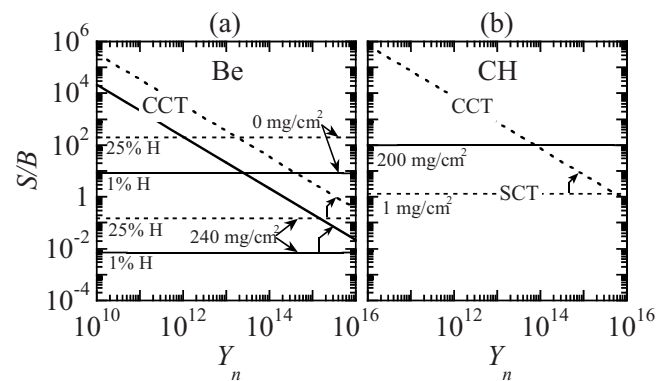


FIG. 8. (a) Signal-to-background (S/B) ratio as a function of Y_n and ρR for ignition-capsule implosions with $\sim 1\%$ residual H (solid lines) and 25%-H-filled Be-capsule implosions (dashed lines). (b) S/B ratios as functions of Y_n for the CH-capsule implosion. The horizontal lines in both figures represent the S/B when a standard-counting technique (SCT) is applied to the data. As shown by the SCT curves, the S/B ratio is independent of Y_n ; a result of the fact that the signal scales with Y_n times the hydrogen content in the fuel for the Be case, or Y_n times the hydrogen content in the ablator for the CH case, while the background scales only with Y_n . A range of S/B ratios of ~ 0.01 –10 and ~ 0.2 –200 is obtained for the failed ignition-capsule implosion with $\sim 1\%$ residual H and 25%-H-filled Be-capsule implosion, respectively; while a S/B ratio varying from ~ 1 to ~ 100 is obtained for the CH-capsule implosion. By applying the coincidence-counting technique (CCT) to the low S/B cases ($S/B \leq 1$), the S/B ratios are improved significantly for $Y_n < 10^{16}$. For neutron yields above 10^{16} , the CCT is not effective due an increased number of background induced random coincidences.

the low S/B cases ($S/B \leq 1$), the S/B ratios are improved significantly for $Y_n < 10^{16}$ as shown in Figs. 8(a) and 8(b).³³ For neutron yields above 10^{16} the CCT is not effective, which is a result of an increased number of random coincidences of neutron-induced tracks on the front and back side of the CR-39. Both in terms of signal and S/B , it is clear that the KO-P measurement technique will be very useful for determining ρR and ρR asymmetries of the remaining ablator for several types of capsule implosions at the NIF.

V. MEASUREMENTS PERFORMED AT OMEGA

Diagnosing shell ρR and ρR asymmetries in gas-filled CH-capsule implosions have been performed routinely at OMEGA for about a decade.^{34–36} In many of those experiments, which are similar to the ablator measurements proposed at the NIF, up to nine charged-particle spectrometers were fielded around an implosion. An example of resulting data from those experiments is illustrated in Fig. 9, which shows a subset of four KO-P spectra obtained from a single high-adiabat implosion involving a capsule with a $27 \mu\text{m}$ CH shell filled with 3 atm of DT gas (shot 39894). ρR 's varying from 20 to $50 \text{ mg}/\text{cm}^2$ were inferred from the Monte Carlo simulated fits (red spectra) to the measured spectra. Very relevant to this work is that Li *et al.* demonstrated in Ref. 34 that these low-mode ρR asymmetries, which are often observed in the charged-particle data obtained at OMEGA, are strongly connected to the laser-power imbalance.

A complementary approach for quickly assessing the ρR value in a certain direction is to look at what energy the KO-P spectrum flattens out; in the case of the $20 \text{ mg}/\text{cm}^2$

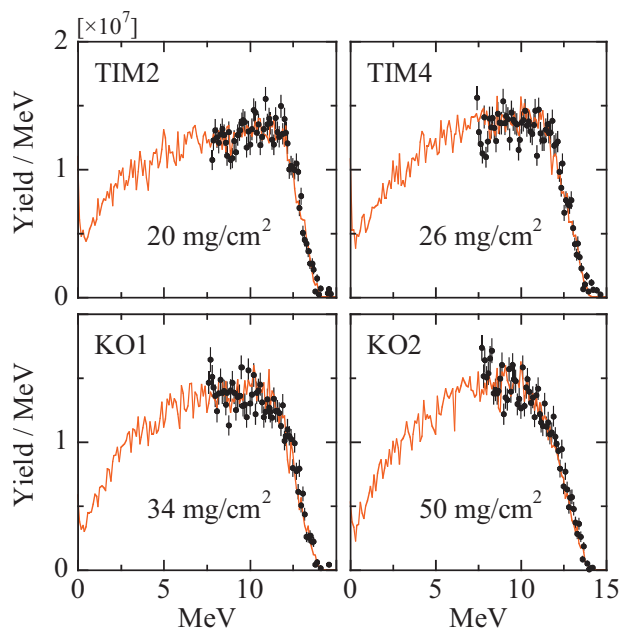


FIG. 9. (Color) A subset of KO-P spectra measured simultaneously in four different directions for OMEGA implosion 39894 (3 atm of DT fuel in a $27 \mu\text{m}$ thick CH shell, illuminated by 60 laser beams delivering 23 kJ of laser energy in a 1-ns square pulse). Narrow-band-width spectrometers that only cover the high-energy portion of the spectrum were used in these measurements. Each spectrum was normalized to the average KO-P yield of 1.5×10^8 . With a measured neutron yield of 6.5×10^{11} , the average S/B ratio is ~ 10 when using the standard counting technique (SCT). The observed differences in the spectral shape are well modeled by steady-state Monte Carlo simulations (red spectra), which indicate significant low-mode ρR modulations, e.g., varying from 20 to 50 mg/cm^2 . A quick assessment of the ρR value in a certain direction can be done by looking at what energy the KO-P spectrum flattens out; for the 20 mg/cm^2 and 50 mg/cm^2 the spectrum flattens out at $\sim 12.5 \text{ MeV}$ and $\sim 10 \text{ MeV}$, respectively.

and 50 mg/cm^2 , the spectrum flattens out at $\sim 12.5 \text{ MeV}$ and $\sim 10 \text{ MeV}$, respectively. The reason for this correlation is best illustrated by using a simple ice-block-implosion model to simulate KO-P spectra for different ρR s of a CH shell. Figure 10(a) shows the ice-block-implosion model used in which the shell density was kept constant (20 g/cc), while the shell thickness was increased in steps of $10 \mu\text{m}$ (a constant electron temperature of 500 eV was used as well). For simplicity a neutron point source at the center of the implosion was also used in these simulations. As shown in Fig. 10(b), the resulting KO-P spectra indicate a strong correlation between the ρR and the energy at which the KO-P spectrum flattens out. Looking at specifically the KO-P spectrum for the 80 mg/cm^2 case, it is now clear that this correlation is a result of the fact that the maximum energy of the escaping KO-Ps produced at, say, $20, 30, 40,$ and $50 \mu\text{m}$ cannot be higher than $9.3, 10.2, 12.5,$ and 14 MeV , respectively.

VI. SUMMARY

We propose to accurately determine the areal density (ρR) of the remaining ablator at bang time for several types of NIF-capsule implosions using charged-particle spectrometry. By fielding several very compact charged-particle spectrometers in different positions around the implosion, ρR and ρR asymmetries of the remaining ablator can be obtained

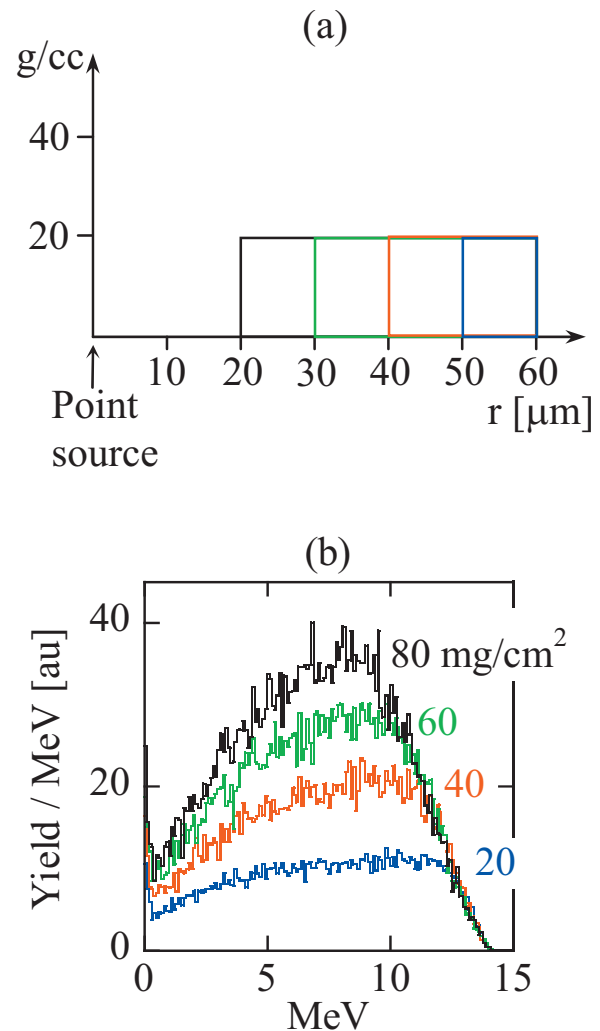


FIG. 10. (Color) Modeling of a capsule implosion, using a simple ice-block-implosion model, to illustrate the relationship between ρR and the shape of the KO-P spectrum. (a) The ice-block-implosion model. A constant shell density of 20 g/cm^3 was used in the model, while the shell thickness was increased in steps of $10 \mu\text{m}$ (a fixed T_e of 500 eV was used as well). A neutron point source at the center of the implosion was also used in these simulations. (b) Simulated KO-P spectra for four different ρR s ranging from 20 to 80 mg/cm^2 . The spectral shapes indicate a strong correlation between the ρR and the energy at which the KO-P spectrum flattens out. Looking at specifically the KO-P spectrum for the 80 mg/cm^2 case, it is clear that this correlation is a result of the fact that the maximum energy of the escaping KO-Ps produced at, say, $20, 30, 40,$ and $50 \mu\text{m}$ cannot be higher than $9.3, 10.2, 12.5,$ and 14 MeV , respectively.

through absolute measurements of yield and spectra of KO-Ps. The results from several simulations of ignition-capsule and H-filled capsule implosions at the NIF and experiments performed at OMEGA clearly indicate that measurements of KO-P spectrum at various locations around an implosion can provide accurate information about ρR and ρR asymmetries of a variety of ablator compositions for neutron yields up to $\sim 6 \times 10^{15}$ and ablator ρR up to $\sim 240 \text{ mg/cm}^2$. In addition, due to the continuous improvements of the spectrometry techniques and CR-39 processing and analysis techniques,³⁷ it is realistic to assume that the ρR of the remaining ablator at bang time can be diagnosed accurately for significantly higher neutron yields than 6×10^{15} .

- ¹G. H. Miller, E. I. Moses, and C. R. Wuest, *Nucl. Fusion* **44**, S228 (2004).
- ²J. D. Lindl, P. Amendt, R. L. Berger, S. G. Glendinning, S. H. Glenzer, S. W. Haan, R. L. Kauffman, O. L. Landen, and L. J. Suter, *Phys. Plasmas* **11**, 339 (2004).
- ³S. W. Haan, M. C. Hermann, T. R. Dittrich, A. J. Fetterman, M. M. Marinak, D. H. Munro, S. M. Pollaine, J. D. Salmonson, G. L. Strobel, and L. J. Suter, *Phys. Plasmas* **12**, 056316 (2005).
- ⁴S. W. Haan, P. A. Amendt, T. R. Dittrich, B. A. Hammel, S. P. Hatchett, M. C. Herrmann, O. A. Hurricane, O. S. Jones, J. D. Lindl, M. M. Marinak, D. Munro, S. M. Pollaine, J. D. Salmonson, G. L. Strobel, and L. J. Suter, *Nucl. Fusion* **44**, S171 (2004).
- ⁵D. H. Munro, P. M. Celliers, G. W. Collins, D. M. Gold, L. B. Da Silva, S. W. Haan, R. C. Cauble, B. A. Hammel, and W. W. Hsing, *Phys. Plasmas* **8**, 2245 (2001).
- ⁶F. H. Séguin, J. A. Frenje, C. K. Li, D. G. Hicks, S. Kurebayashi, J. R. Rygg, B.-E. Schwartz, and R. D. Petrasso, S. Roberts, J. M. Soures, D. D. Meyerhofer, T. C. Sangster, J. P. Knauer, C. Sorce, V. Yu. Glebov, C. Stoeckl, T. W. Phillips, R. J. Leeper, K. Fletcher, and S. Padalino, *Rev. Sci. Instrum.* **74**, 975 (2003).
- ⁷S. P. Hatchett explored the idea of using knock-on deuterons (KO-D) to diagnose the beryllium ablator. However, it turned out that this was not feasible as the KO-Ds have a relatively short range.
- ⁸S. Kurebayashi, J. A. Frenje, F. H. Séguin, J. R. Rygg, C. K. Li, R. D. Petrasso, V. Yu. Glebov, J. A. Delettrez, T. C. Sangster, D. D. Meyerhofer, C. Stoeckl, J. M. Soures, P. A. Amendt, S. P. Hatchett, and R. E. Turner, *Phys. Plasmas* **12**, 032703 (2005).
- ⁹C. K. Li and R. D. Petrasso, *Phys. Rev. Lett.* **70**, 3059 (1993).
- ¹⁰As this ρR value is smaller than the predicted value for a perfectly driven implosion ($\sim 400 \text{ mg/cm}^2$), the KO-P technique will be used primarily to diagnose over-driven implosions, effects of power imbalance, and possibly to address the effect of the Rayleigh–Taylor growth at the fuel-ablator interface.
- ¹¹H. Nakaishi, N. Miyana, H. Azechi, M. Yamanaka, T. Yamanaka, M. Takagi, T. Jitsuno, and S. Nakai, *Appl. Phys. Lett.* **54**, 1308 (1989).
- ¹²C. K. Li, F. H. Séguin, D. G. Hicks, J. A. Frenje, K. M. Green, S. Kurebayashi, R. D. Petrasso, D. D. Meyerhofer, J. M. Soures, V. Yu. Glebov, R. L. Keck, P. B. Radha, S. Roberts, W. Seka, S. Skupsky, C. Stoeckl, and T. C. Sangster, *Phys. Plasmas* **8**, 4902 (2001).
- ¹³J. A. Frenje, C. K. Li, F. H. Séguin, S. Kurebayashi, R. D. Petrasso, J. M. Soures, J. Delettrez, V. Yu. Glebov, D. D. Meyerhofer, P. B. Radha, S. Roberts, T. C. Sangster, S. Skupsky, and C. Stoeckl, *Phys. Plasmas* **9**, 4719 (2002).
- ¹⁴F. H. Séguin, C. K. Li, J. A. Frenje, S. Kurebayashi, R. D. Petrasso, F. J. Marshall, D. D. Meyerhofer, J. M. Soures, T. C. Sangster, C. Stoeckl, J. A. Delettrez, P. B. Radha, V. A. Smalyuk, and S. Roberts, *Phys. Plasmas* **9**, 3558 (2002).
- ¹⁵D. G. Hicks, C. K. Li, F. H. Séguin, A. K. Ram, J. A. Frenje, R. D. Petrasso, J. M. Soures, V. Yu. Glebov, D. D. Meyerhofer, S. Roberts, C. Sorce, and C. Stoeckl, T. C. Sangster, and T. W. Phillips, *Phys. Plasmas* **7**, 5106 (2000).
- ¹⁶D. C. Wilson, R. L. Singleton, Jr., J. P. Grondalski, N. M. Hoffman, A. Nobile, Jr., F. H. Séguin, J. A. Frenje, C. K. Li, and R. D. Petrasso, *Rev. Sci. Instrum.* **77**, 10E711 (2006).
- ¹⁷D. G. Hicks, B. Spears, C. Sorce, P. Celliers, O. Landen, G. Collins, and T. Boehly, *Bull. Am. Phys. Soc.* **52**, 65 (2007).
- ¹⁸R. E. Olson, G. A. Rochau, and R. J. Leeper, *Bull. Am. Phys. Soc.* **52**, 65 (2007).
- ¹⁹R. E. Olson, R. J. Leeper, A. Nobile, J. A. Oertel, G. A. Chandler, K. Cochrane, S. C. Dropinski, S. Evans, S. W. Haan, J. L. Kaae, J. P. Knauer, K. Lash, L. P. Mix, A. Nikroo, G. A. Rochau, G. Rivera, C. Russell, D. Schroen, R. J. Sebring, D. L. Tanner, R. E. Turner, and R. J. Wallace, *Phys. Plasmas* **11**, 2778 (2004).
- ²⁰C. K. Li, D. G. Hicks, F. H. Séguin, J. A. Frenje, R. D. Petrasso, J. M. Soures, P. B. Radha, V. Yu. Glebov, C. Stoeckl, D. R. Harding, J. P. Knauer, R. Kremens, F. J. Marshall, D. D. Meyerhofer, S. Skupsky, S. Roberts, C. Sorce, T. C. Sangster, T. W. Phillips, and M. D. Cable, *Phys. Plasmas* **7**, 2578 (2000).
- ²¹S. W. Haan, P. A. Amendt, D. A. Callahan, T. R. Dittrich, M. J. Edwards, B. A. Hammel, D. D. Ho, O. S. Jones, J. D. Lindl, M. M. Marinak, D. H. Munro, S. M. Pollaine, J. D. Salmonson, B. K. Spears, and L. J. Suter, *Fusion Sci. Technol.* **51**, 509 (2007).
- ²²S. W. Haan, P. A. Amendt, D. A. Callahan, M. C. Herrmann, P. A. Amendt, D. A. Callahan, T. R. Dittrich, M. J. Edwards, O. S. Jones, M. M. Marinak, D. H. Munro, S. M. Pollaine, J. D. Salmonson, B. K. Spears, and L. J. Suter, *Fusion Sci. Technol.* **49**, 553 (2006).
- ²³A. Nikroo, K. C. Chen, M. L. Hoppe, H. Huang, J. R. Wall, H. Xu, M. W. McElfresh, C. S. Alford, R. C. Cook, J. C. Cooley, R. Fields, R. Hackenberg, R. P. Doerner, and M. Baldwin, *Phys. Plasmas* **13**, 056302 (2006).
- ²⁴J. Biener, P. B. Mirkarimi, J. W. Tringe, S. L. Baker, Y. Wang, S. O. Kucheyev, N. E. Teslich, K. J. J. Wu, A. V. Hamza, C. Wild, E. Woerner, P. Koidl, K. Bruehne, and H.-J. Fecht, *Fusion Sci. Technol.* **49**, 737 (2006).
- ²⁵The diamond-ablator design can, in principle, be diagnosed using the same method as that of Be.
- ²⁶R. D. Petrasso, C. K. Li, M. D. Cable, S. M. Pollaine, S. W. Haan, T. P. Bernat, J. D. Kilkenny, S. Cremer, J. P. Knauer, C. P. Verdon, and R. L. Kremens, *Phys. Rev. Lett.* **77**, 2718 (1996).
- ²⁷The effect of fuel-ablator mix results in a ρR value that reflects the clean ablator.
- ²⁸J. Delettrez, *Can. J. Phys.* **64**, 932 (1986).
- ²⁹As CR-39 detectors are used in the proton spectrometers, the signal (S) scales with hydrogen content in the fuel times primary neutron yield (Y_n) (Ref. 20) while the background (B), which is mainly due to neutrons, only scales with Y_n (Ref. 30). As a result, the S/B ratio increases with increasing hydrogen content in the fuel.
- ³⁰J. A. Frenje, C. K. Li, F. H. Séguin, D. G. Hicks, S. Kurebayashi, R. D. Petrasso, S. Roberts, V. Yu. Glebov, D. D. Meyerhofer, T. C. Sangster, J. M. Soures, C. Stoeckl, C. Chiriac, G. J. Schmid, and R. A. Lerche, *Rev. Sci. Instrum.* **73**, 2597 (2002).
- ³¹D. T. Casey, J. A. Frenje, S. C. McDuffee, C. K. Li, J. R. Rygg, F. H. Séguin, R. D. Petrasso, V. Yu. Glebov, D. D. Meyerhofer, S. Roberts, and T. C. Sangster, *Bull. Am. Phys. Soc.* **52**, 208 (2007).
- ³²D. T. Casey, J. A. Frenje, C. K. Li, J. R. Rygg, C. K. Li, S. C. McDuffee, M. Manuel, R. D. Petrasso, V. Yu. Glebov, T. C. Sangster, D. D. Meyerhofer, S. Roberts, P. Song, and M. Moran, "Minimizing background at the Magnetic Recoil Spectrometer (MRS) at OMEGA and the National Ignition Facility (NIF)," *Rev. Sci. Instrum.* (to be published).
- ³³The CCT utilizes the fact that a signal event produces a track on both the front and back side of a thin piece of CR-39, while a neutron-background event produces only a track on either the front or back side of the CR-39. By correlating the front and back side scans of the CR-39 data, most of the background is rejected, which significantly improves the S/B .
- ³⁴C. K. Li, F. H. Séguin, J. A. Frenje, R. D. Petrasso, R. Rygg, S. Kurebayashi, B. Schwartz, R. L. Keck, J. A. Delettrez, J. M. Soures, P. W. McKenty, V. N. Goncharov, J. P. Knauer, F. J. Marshall, D. D. Meyerhofer, P. B. Radha, S. P. Regan, T. C. Sangster, W. Seka, and C. Stoeckl, *Phys. Plasmas* **10**, 1919 (2003).
- ³⁵J. A. Frenje, C. K. Li, F. H. Séguin, J. Deciantis, S. Kurebayashi, J. R. Rygg, R. D. Petrasso, J. Delettrez, V. Yu. Glebov, C. Stoeckl, F. J. Marshall, D. D. Meyerhofer, T. C. Sangster, V. A. Smalyuk, and J. M. Soures, *Phys. Plasmas* **11**, 2798 (2004).
- ³⁶C. K. Li, F. H. Séguin, J. A. Frenje, R. D. Petrasso, J. A. Delettrez, P. W. McKenty, T. C. Sangster, R. L. Keck, J. M. Soures, F. J. Marshall, D. D. Meyerhofer, V. N. Goncharov, J. P. Knauer, P. B. Radha, S. P. Regan, and W. Seka, *Phys. Rev. Lett.* **92**, 205001 (2004).
- ³⁷S. C. McDuffee, J. A. Frenje, F. H. Séguin, R. Leiter, M. J. Canavan, D. T. Casey, J. R. Rygg, C. K. Li, and R. D. Petrasso, *Rev. Sci. Instrum.* **79**, 043302 (2008).